Vertically-Ordered Mesoporous Silica Films Grown on Boron Nitride-Graphene Composite Modified Electrodes for Rapid and Sensitive Detection of Carbendazim in Real Samples

Yanqi Zou[1], Xiaoyu Zhou[1], Liuhong Xie[2], Hongliang Tang[3]* and Fei Yan[1]*

[1]Key Laboratory of Surface & Interface Science of Polymer Materials of Zhejiang Province, Department of Chemistry, Zhejiang Sci-Tech University, Hangzhou, China, [2]The First Clinical Faculty of Guangxi University of Chinese Medicine, Nanning, China, [3]Affiliated Fangchenggang Hospital, Guangxi University of Chinese Medicine, Fangchenggang, China

Carbendazim (CBZ), a kind of widely used pesticide, is harmful to human health and environmental ecology. Therefore, it is of great importance to detect CBZ in real samples. Herein we report the stable growth of vertically-ordered mesoporous silica films (VMSF) on the glassy carbon electrode (GCE) using boron nitride-reduced graphene oxide (BN-rGO) nanocomposite as an adhesive and electroactive layer. Oxygen-containing groups of rGO and 2D planar structure of BN-rGO hybrid favor the stable growth of VMSF via the electrochemically assisted self-assembly (EASA) method. Combining the good electrocatalytic activity of BN-rGO and the enrichment effect of VMSF, the proposed VMSF/BN-rGO/GCE can detect CBZ with high sensitivity (3.70 µA/µM), a wide linear range (5 nM–7 µM) and a low limit of detection (2 nM). Furthermore, due to the inherent anti-fouling and anti-interference capacity of VMSF, direct and rapid electrochemical analyses of CBZ in pond water and grape juice samples are also achieved without the use of complicated sample treatment processes.

Keywords: vertically-ordered mesoporous silica films, boron nitride, graphene, carbendazim, electrochemical sensors, anti-fouling detection

INTRODUCTION

As a low-cost pesticide with broad spectrum activity, carbendazim (CBZ) plays a key role in controlling pests and diseases or weeds in agricultural production (Wei et al., 2018). Due to the stable characteristic of the benzimidazole ring, CBZ is stable and difficult to degrade. With the extensive and uncontrolled use of CBZ, the accumulation of CBZ residues can be found in the environment (e.g., soil and water), which may result in the long-term adverse effects on the ecological safety and water ecosystem (Ghorbani et al., 2021; Baigorria and Fraceto, 2022). Moreover, CBZ will cause serious health effects through the respiratory system and direct contacts, such as skin inflammation, eye irritation, disruption of the endocrine system, and hormonal disorder (Zhu et al., 2019; Farooq et al., 2020; Rai and Mercurio, 2020). Therefore, highly sensitive and accurate detection of CBZ in the environment is of significance for human health and environmental protection.

At present, sorts of methods for detecting CBZ have been developed, for example, mass spectrometry (Grujic et al., 2005), UV-vis spectroscopy (Pourreza et al., 2015), surface-enhanced Raman scattering (SERS) (Furini et al., 2015), gas chromatography (Lesueur et al., 2008), and high-performance liquid chromatography (Yamaguchi et al., 2011; Subhani et al., 2013). However, these techniques inevitably need expensive equipment, complex sample pretreatment steps, and a long analysis cycle (Yang et al., 2018). By contrast, the electrochemical method has the advantages of high sensitivity, low cost, rapidity, and convenient operation (Govindasamy et al., 2017a; Govindasamy et al., 2017b; Akilarasan et al., 2018; Keerthi et al., 2018), which has been applied for CBZ determination (Mekeuo et al., 2021). Due to the electrode fouling caused by the undesirable adsorption of biological macromolecules or microorganisms, complicated pretreatments of real samples are often required for electrochemical sensors and inevitably produce damage to the analytes. Therefore, designing anti-fouling and anti-interference electrode interfaces for direct electrochemical analysis of complex real samples is greatly important (Zhou et al., 2020).

Porous materials have aroused growing attention in the construction of rapid and portable sensors (Cui et al., 2020; Cui et al., 2021; Duan et al., 2021; Liu et al., 2022; Wei et al., 2022). Especially, vertically-ordered mesoporous silica films (VMSF) are a kind of porous material with perpendicularly ordered nanochannels and uniform pore size on a nanometer scale (Walcarius, 2021; Ma et al., 2022a). VMSF has advantages of high permeability, molecular selectivity, molecular sieving, insulation, and good mechanical and chemical stability, which has been widely employed as the anti-fouling coating for direct electrochemical analysis (Yan and Su, 2016; Huaxu Zhou et al., 2021). Arising from the high density of silanol groups on the channel walls and ultrasmall size of channels, molecular selectivity, and performance of VMSF could be modulated by modification of functional groups and confined growth of nanomaterials, broadening its practical applications (Lu et al., 2018; Yan et al., 2020a). For example, graphene quantum dots (GQD), a 0D graphene materials (Yan et al., 2019), are characterized by an atomically thin planar carbon structure with ultrasmall size (He et al., 2019; Mao et al., 2019), abundant active sites (Kaixin Li et al., 2018; Ge et al., 2019; Wan et al., 2021), tunable chemicophysical properties (Nan Li et al., 2018; Pang et al., 2018; Yan et al., 2018), and efficient heterogeneous electron transfer capacity (Huang et al., 2018; Tian et al., 2018; Gong et al., 2021a), could be confined into the nanochannels of VMSF to serve as the recognition, enrichment, and catalysis element, leading to the ultrasensitive electrochemical analysis of heavy metal ions and neurotransmitter in complex real samples (Lu et al., 2018). Currently, VMSF supported by indium tin oxide (ITO) electrode is rather stable and could be fabricated by using electrochemically-assisted self-assembly (EASA) and Stöber-solution approaches (Zhou et al., 2019; Walcarius, 2021). Premodification of molecular glues [e.g., organosilanes (Nasir et al., 2018; Gong et al., 2021b) or reduced graphene oxide (rGO) nanosheets (Yan et al., 2020b; Ma et al., 2022b)] and pretreatment

process [e.g., electro-activation (Xuan et al., 2021; Wang et al., 2022) or plasma (Zhu et al., 2022)] can stably prepare VMSF on the other commercial conductive electrodes (e.g., metal electrode or carbonaceous electrode). As our group reported recently, the introduction of rGO as an adhesive and electroactive layer onto the electrode surface is capable of maintaining the well-oriented nanochannel structures of VMSF and greatly improving the sensitivity and selectivity of electrochemical sensors (Xi et al., 2019; Yan et al., 2021). Note that rGO hybrids with functional materials have been reported to further extend the scope of analytes (Kogularasu et al., 2017; Muthumariappan et al., 2017) and provide a versatile platform for VMSF-graphene-based electrochemical sensing platform (Lin Zhou et al., 2021; Zhou et al., 2022).

Thanks to the similar 2D planar structure to graphene, boron nitride (BN) has received more attention and it has several advantages of high specific surface area, good chemical and thermal stability, and excellent catalytic activity (Weng et al., 2016; Wang et al., 2021). Although the bulk BN is electrically insulating, the hybrid of graphene and BN could exhibit excellent electrochemical properties due to the smaller band gap (Qun Li et al., 2018). In this work, we report that VMSF could be stably grown onto the GCE by using a hybrid of BN and reduced graphene oxide (BN-rGO) as the adhesive and electroactive layer. BN-rGO modified GCE provides oxygen-containing groups, hydrophobic π-conjugated structure, and relatively planar substrate, favoring the stable growth of VMSF. And the obtained VMSF/BN-rGO/GCE displays good electrochemical performance to CBZ with high sensitivity and a low detection limit, owing to the excellent electrochemical activity of BN-rGO and enrichment effect of VMSF through strong hydrogen bonding. Furthermore, due to the excellent anti-fouling and anti-interference ability of VMSF, direct electrochemical analysis of CBZ in pond water and grape juice samples was achieved with good stability.

MATERIALS AND METHODS

Chemical and Materials

All chemicals and reagents of analytical grade were used as received without further purification. And ultrapure water (18.2 MΩ cm) was used to prepare all aqueous solutions throughout this work. GO aqueous solution (1 mg/ml) was supplied from Hangzhou Gaoxi Tech. Boron nitride (99.9%), carbendazim (CBZ, 97%), Sodium phosphate monobasic dihydrate ($NaH_2PO_4.2H_2O$, 99%), cetyltrimethylammonium bromide (CTAB), tetraethoxysilane (TEOS, 98%), potassium hydrogen phthalate (KHP, 99.8%), potassium ferricyanide (K_3[Fe(CN)$_6$], 99.5%), humic acid (HA, 90%), starch soluble (Starch, 99%), hematin porcine (Heme, 95%), albumin from bovine serum (BSA, 96%), lauryl sodium sulfate (SDS, 98.5%) were gotten from Aladdin. Sodium phosphate dibasic dodecahydrate ($Na_2HPO_4.12H_2O$, 99%) was obtained from Macklin. Lignin alkali was received from Solarbio. Sodium nitrate ($NaNO_3$) was purchased from Wuxi Zhangwang Chemical Reagent. Hexaammineruthenium (III) chloride ($Ru(NH_3)_6Cl_3$, 98%) was

SCHEME 1 | Illustration of the preparation of VMSF/BN-rGO/GCE electrode.
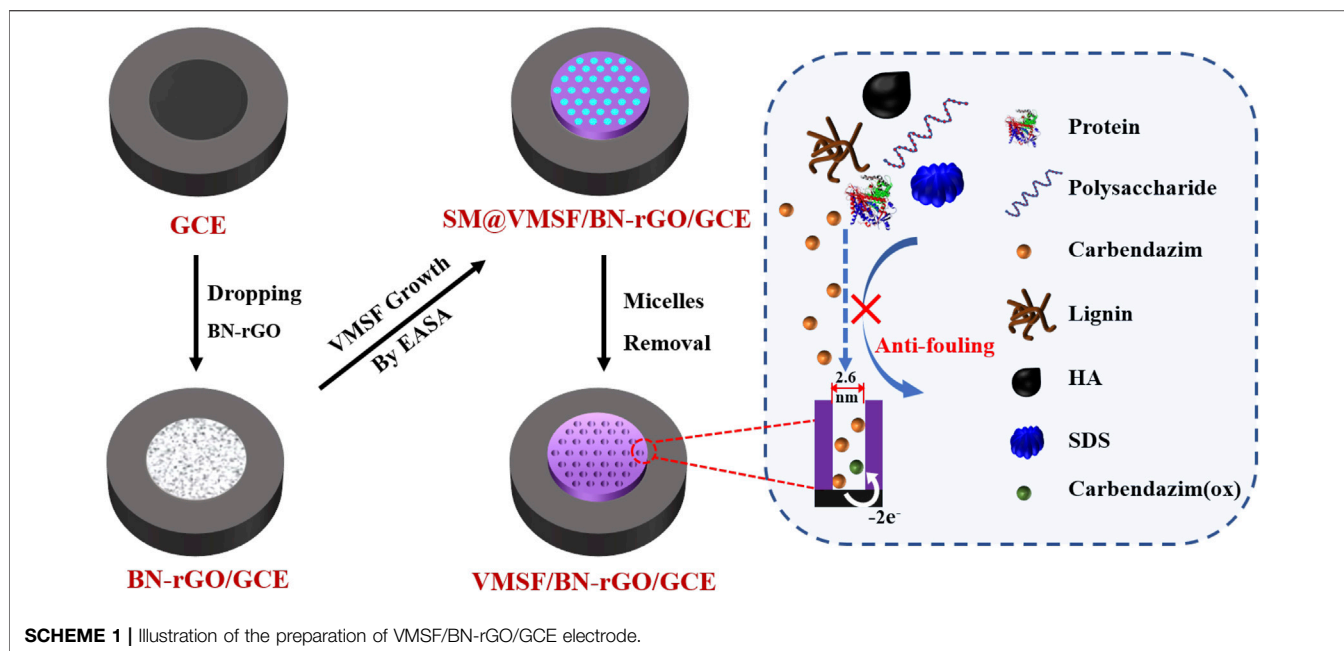
purchased from Sigma. Potassium chloride (KCl, 99.5%), calcium chloride (CaCl$_2$, 95%), natrium bicarbonate (NaHCO$_3$, 95%), sodium chloride (NaCl, 99.5%), magnesium chloride (MgCl$_2$, 95%), potassium dihydrogen phosphate (KH$_2$PO$_4$, 99%) were obtained from Hangzhou Gaojing Fine Chemical Reagent. Pond water was obtained from the campus of Zhejiang Sci-Tech University. Grape juice was bought from supermarkets.

Measurements and Instrumentations

X-Photoelectron spectroscopy (XPS) data was obtained from PHI5300 electron spectrometer (PE Ltd., United States) at 250 W, 14 kV, MgK α radiation. A transmission electron microscopy (TEM) image was collected from an HT7700 microscope (Hitachi, Japan) at an acceleration voltage of 100 kV. Cyclic voltammetry (CV) and differential pulse voltammetry (DPV) tests were performed on an Autolab (PGSTAT302N) electrochemical workstation (Metrohm, Switzerland) at room temperature. A routine three-electrode system was used, with Ag/AgCl (saturated with KCl) as the reference electrode, platinum electrode as the counter electrode, bare GCE, or modified GCE as the working electrode. The DPV arguments were as follows: step potential, 0.005 V; pulse time, 0.05 s; pulse amplitude, 0.05 V; interval time, 0.2 s.

Synthesis of BN-rGO Dispersion

Boron nitride nanosheets (BN) were prepared according to the method previously reported with slight modification (Du et al., 2013). Briefly, 0.1 g of original boron nitride powder was dispersed into 5 ml H$_2$SO$_4$ (98%, w/w) and stirred for 30 min. Then, 0.1 g KMnO$_4$ was added to the aforementioned solution at 0°C and stirred for another 12 h. After the addition of 0.5 ml of H$_2$O$_2$ (30%, w/w), the resulting suspension was centrifuged at 3,000 rpm for 5 min to remove the supernatant. After being washed with water and baked at 40°C for 24 h, BN was obtained.

0.0002 g BN was dispersed in 20 ml GO (0.1 mg/ml) solution and ultrasonicated for 0.5 h. Then, 60 μL ammonia water and 6 μL hydrazine hydrate (50%, w/w) were added to the aforementioned dispersion, followed by incubation in an aqueous bath at 60°C for 3.5 h. The obtained mixture was centrifuged at 3,000 rpm for 5 min, and the supernatant was taken to obtain the BN-rGO dispersion.
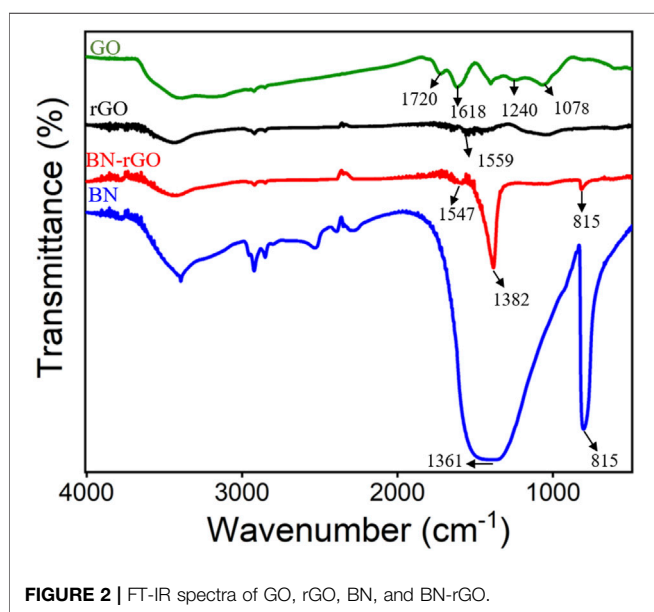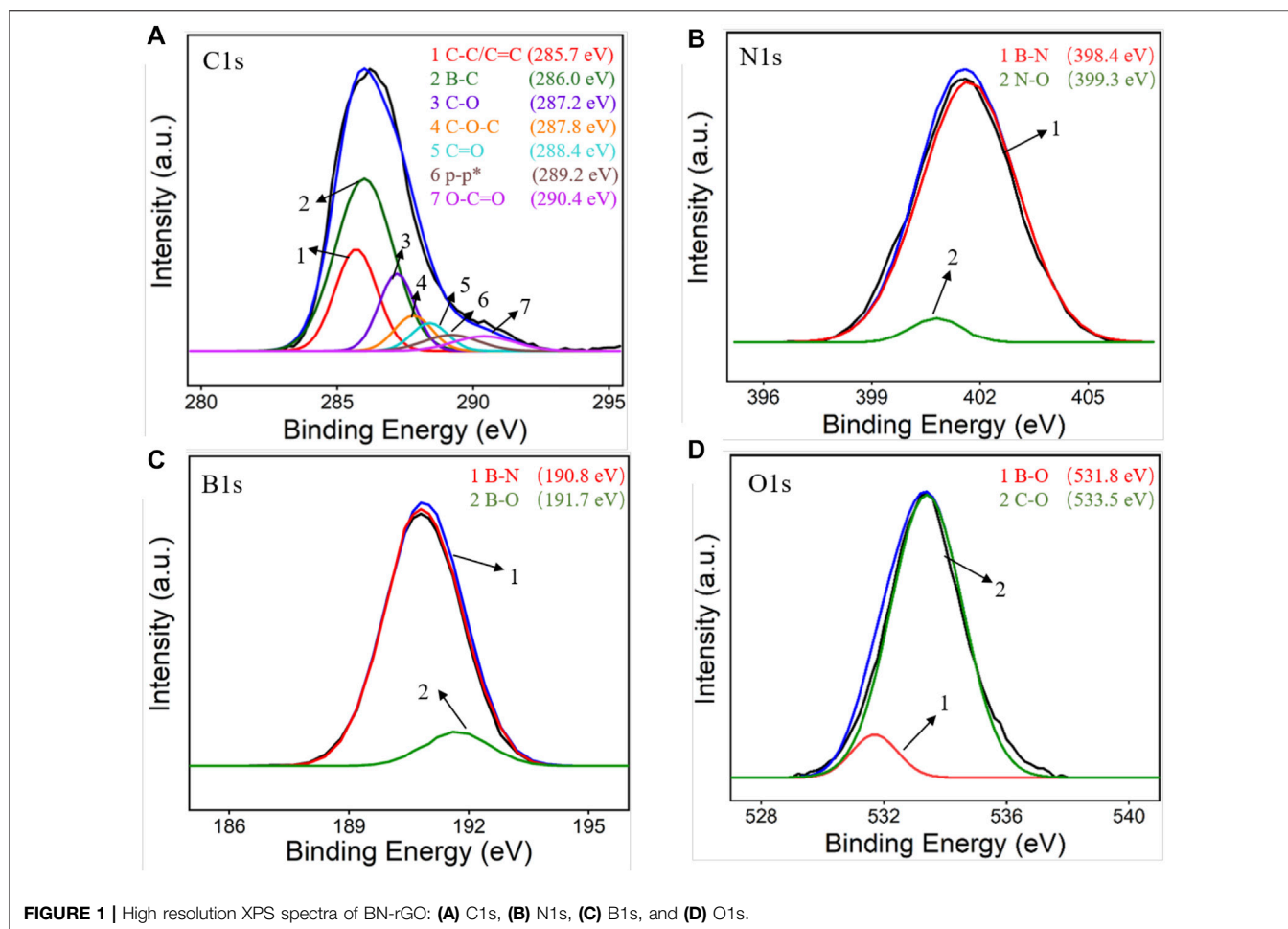
Preparation of the VMSF/BN-rGO/GCE

Prior to the electrode modification, GCE (3 mm diameter) was polished with 0.3 and 0.05 μm alumina powder, and then ultrasonically cleaned with absolute alcohol and distilled water. An illustration of the preparation of the VMSF/BN-rGO/GCE electrode is displayed in **Scheme 1**. As seen, 5 μl BN-rGO dispersion was primarily dropped onto a freshly cleaned GCE, and dried at 60°C. The resulting electrode was named BN-rGO/GCE. Then the VMSF was prepared on the BN-rGO/GCE by using the electrochemically assisted self-assembly (EASA) as previously reported (Xi et al., 2019). Briefly, a constant potential (−2.2 V) was applied to the BN-rGO/GCE for 5 s. After being aged at 80°C for 10 h, VMSF with the surfactant micelles (SM) inside the nanochannels was grown on the BN-rGO/GCE, termed as SM@VMSF/BN-rGO/GCE. Removal of SM could be performed by immersing the SM@VMSF/BN-rGO/GCE into the 0.1 M HCl-ethanol solution under moderate stirring for 5 min, to obtain VMSF/BN-rGO/GCE.

RESULTS AND DISCUSSION

Characterization of VMSF/BN-rGO/GCE

XPS was first employed to characterize the BN-rGO composite and the results were shown in **Figure 1**. As revealed in **Figure 1A**, there exist seven characteristic carbon 1 s XPS peaks located at 285.7,

FIGURE 1 | High resolution XPS spectra of BN-rGO: **(A)** C1s, **(B)** N1s, **(C)** B1s, and **(D)** O1s.

FIGURE 2 | FT-IR spectra of GO, rGO, BN, and BN-rGO.

286.0, 287.2, 287.8, 288.4, 289.2, and 290.4 eV, which are assigned to C-C/C=C, B-C, C-O, C-O-C, C=O, π-π^* bond and O-C=O bond, respectively. Two obvious nitrogen 1 s XPS peaks were observed at 398.4 and 399.3 eV (**Figure 1B**), corresponding to B-N and N-O bonds, respectively. The B-N and B-O bonds of boron 1s produce two XPS peaks at 190.8 and 191.7 eV (**Figure 1C**). And two oxygen 1s XPS peaks corresponding to the B-O and C-O bonds are displayed at 531.8 and 533.5 eV. **Figure 2** depicts the FT-IR spectra of the BN-rGO composite. It could be found that GO has four characteristic peaks at ~1,078 cm^{-1} (C-O), ~1,240 cm^{-1} (C-O-C), and ~1,618 cm^{-1} (C=C), and ~1720 cm^{-1} (C=O). After the chemical reduction of GO to rGO, intensities of oxygen-containing groups remarkably decrease and an absorption peak at ~1,559 cm^{-1} (C=O) is observed. In comparison with BN and rGO, BN-rGO nanocomposite possesses characteristic absorption bands of BN at 815 cm^{-1} (B-N), ~1,382 cm^{-1} (B-N-B), and that of rGO at 1,547 cm^{-1} (C-O), showing the successful preparation of BN-rGO nanocomposite.

VMSF was grown onto the BN-rGO/GCE by using the EASA method (Xi et al., 2019) and its morphology was characterized by
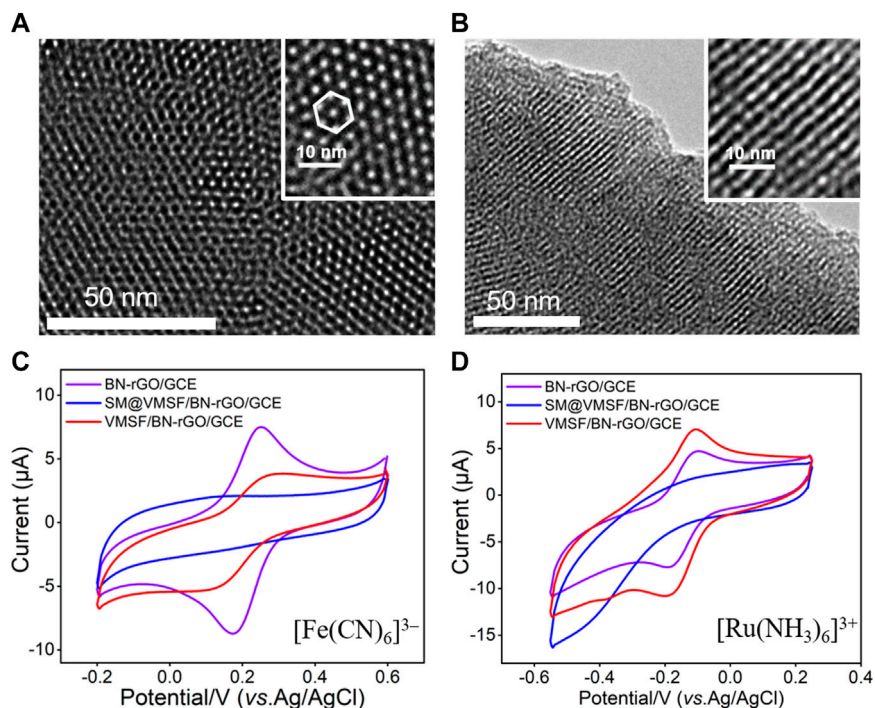
FIGURE 3 | Top-view (A) and cross-sectional view (B) TEM images of VMSF. The insets are corresponding magnified images. CV curves obtained from the BN-rGO/GCE, SM@VMSF/BN-rGO/GCE and VMSF/BN-rGO/GCE electrodes in 0.05 M KHP containing 0.5 mM $[Fe(CN)_6]^{3-}$ (C) and $[Ru(NH_3)_6]^{3+}$ (D). The scan rate was 50 mV/s.
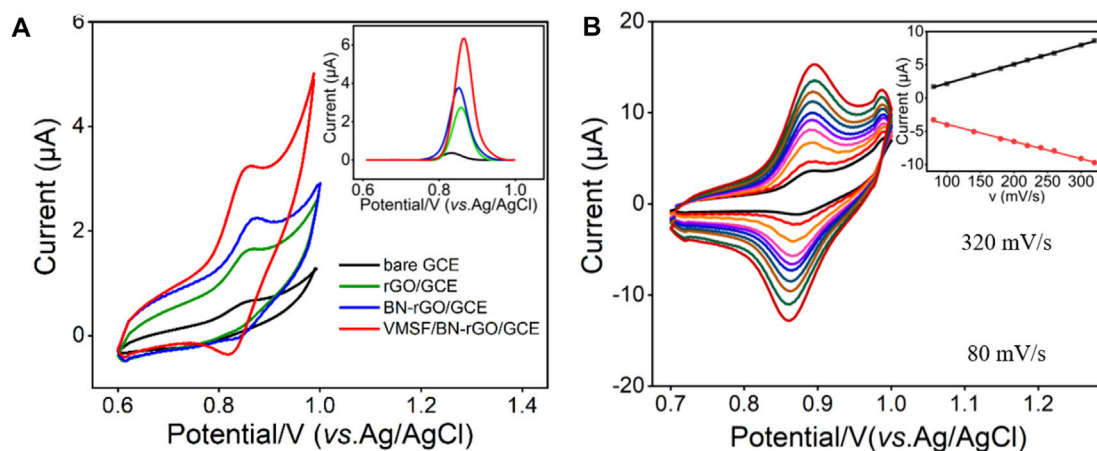


FIGURE 4 | (A) CV curves obtained from the bare GCE, rGO/GCE, BN-rGO/GCE, and VMSF/BN-rGO/GCE electrodes in 0.1 M PBS (pH 6.0) containing 1 μM CBZ. Inset is the corresponding DPV curves. The scan rate was 50 mV/s. (B) CV curves of 1 μM CBZ in 0.1 M PBS (pH 6.0) at the VMSF/BN-rGO/GCE at different scan rates (80–320 mV s^{-1}). The inset is the relationship between the oxidation peak currents and scan rates.

TEM. It can be seen from the top-view TEM image that VMSF has hexagonal and regular nanopores with a uniform pore diameter of 2.6 nm (**Figure 3A**). And cross-sectional TEM image reveals that the nanochannels of VMSF are perpendicularly oriented and parallel to each other (**Figure 3B**). The integrity and permeability of VMSF were

investigated by cyclic voltammetry (CV) using two kinds of conventional charged electrochemical probes, namely positively charged $Ru(NH_3)_6^{3+}$ and negatively charged $Fe(CN)_6^{3-}$. As shown in **Figures 3C, D**, no obvious redox signals for both $Ru(NH_3)_6^{3+}$ and $Fe(CN)_6^{3-}$ are observed at the SM@VMSF/BN-rGO/GCE, which is due to the
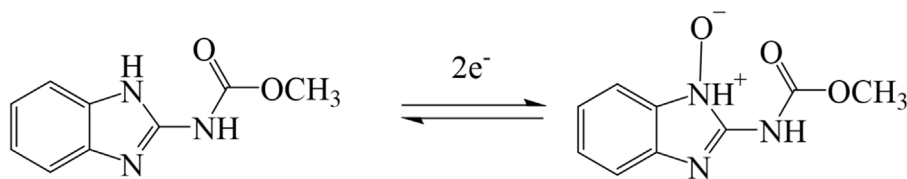
SCHEME 2 | Electrochemical reaction mechanism of CBZ.
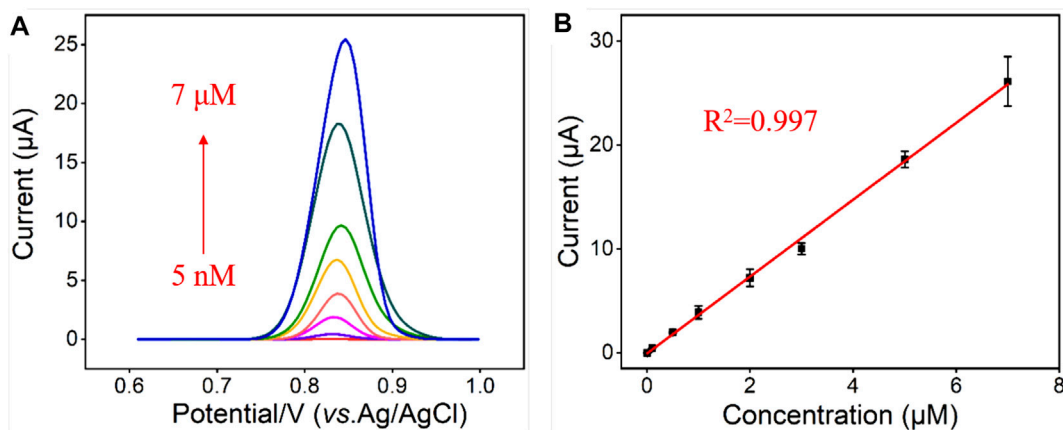
FIGURE 5 | (A) DPV curves obtained from the VMSF/BN-rGO/GCE in response to different concentrations of CBZ (0.005, 0.01, 0.1, 0.5, 1, 2, 3, 5 and 7 µM). The supporting electrolyte is 0.1 M PBS (pH 6.0); Inset is amplified DPV curves. **(B)** Calibration plot for CBZ. The error bars represent the standard deviation (SD) of three measurements.

TABLE 1 | Comparison of the analytical performances of various analytical methods for the determination of CBZ.

| Materials	Method	Range (µM)	LOD (µM)	Ref
N, P-CQDs, and Au NPs	FL	0.005–1.57	0.002	Yang et al. (2018)
N-CQDs/AuNCs	FL	1–100	0.83	Yang et al. (2020)
	SERS	150–1,000	37.85	
SAX/PSA	HPLC-UV	0.26–1.57	0.015	Phansawan et al. (2015)
NPG/GCE	Electrochemistry	10–70	0.24	Gao et al. (2019)
CMC-MWCNTs/GCE	Electrochemistry	0.03–10	0.015	Zhou et al. (2018)
CPE/FS@Ag	Electrochemistry	0.05–10	0.00094	Ozcan et al. (2021)
NP-Cu/rGO/GCE	Electrochemistry	0.5–30	0.09	Tian et al. (2019)
VMSF/BN-rGO/GCE	Electrochemistry	0.005–7	0.002	This work

N, P-CQDs: N, P-doped carbon quantum dots; Au NPs: FL, fluorescence; gold nanoparticles; N-CQDs: nitrogen-doped carbon quantum dots; AuNCs: gold nanocluster; SAX/PSA: strong anion exchange/primary secondary amine; NPG: nanoporous gold; CMC: carboxymethyl cellulose; MWCNTs: multi-walled carbon nanotube; CPE: carbon paste electrode; FS: silver nanoparticles on fumed silica; NP-Cu: nanoporous copper.

impermeable SM inside the nanochannels of VMSF and further indicates the obtained VMSF onto the BN-rGO/GCE is intact. After the extraction of SM from the nanochannels, electrochemical signals of two charged probes are recovered to a certain extent at the VMSF/BN-rGO/GCE. And VMSF/BN-rGO/GCE displays apparent charge permselectivity, namely attracting $Ru(NH_3)_6^{3+}$ and repelling $Fe(CN)_6^{3-}$, compared to the BN-rGO/GCE. This is because silanol groups onto the inner walls of VMSF are deprotonated to produce a negative charge under the experimental condition. Note that the current magnitude of $Ru(NH_3)_6^{3+}$ at the VMSF/BN-rGO/GCE is

comparable to that of the BN-rGO/GCE, suggesting the high permeability of VMSF.

Electrochemical Behavior of VMSF/ BN-rGO/GCE

In order to testify the detection performance, CV and DPV responses of 1 µM CBZ at the bare GCE, rGO/GCE, BN-rGO/GCE, and VMSF/BN-rGO/GCE were compared in **Figure 4A**. As shown, CBZ can produce weak redox peaks at the bare GCE electrode, corresponding to the redox reaction of CBZ (**Scheme 2**)
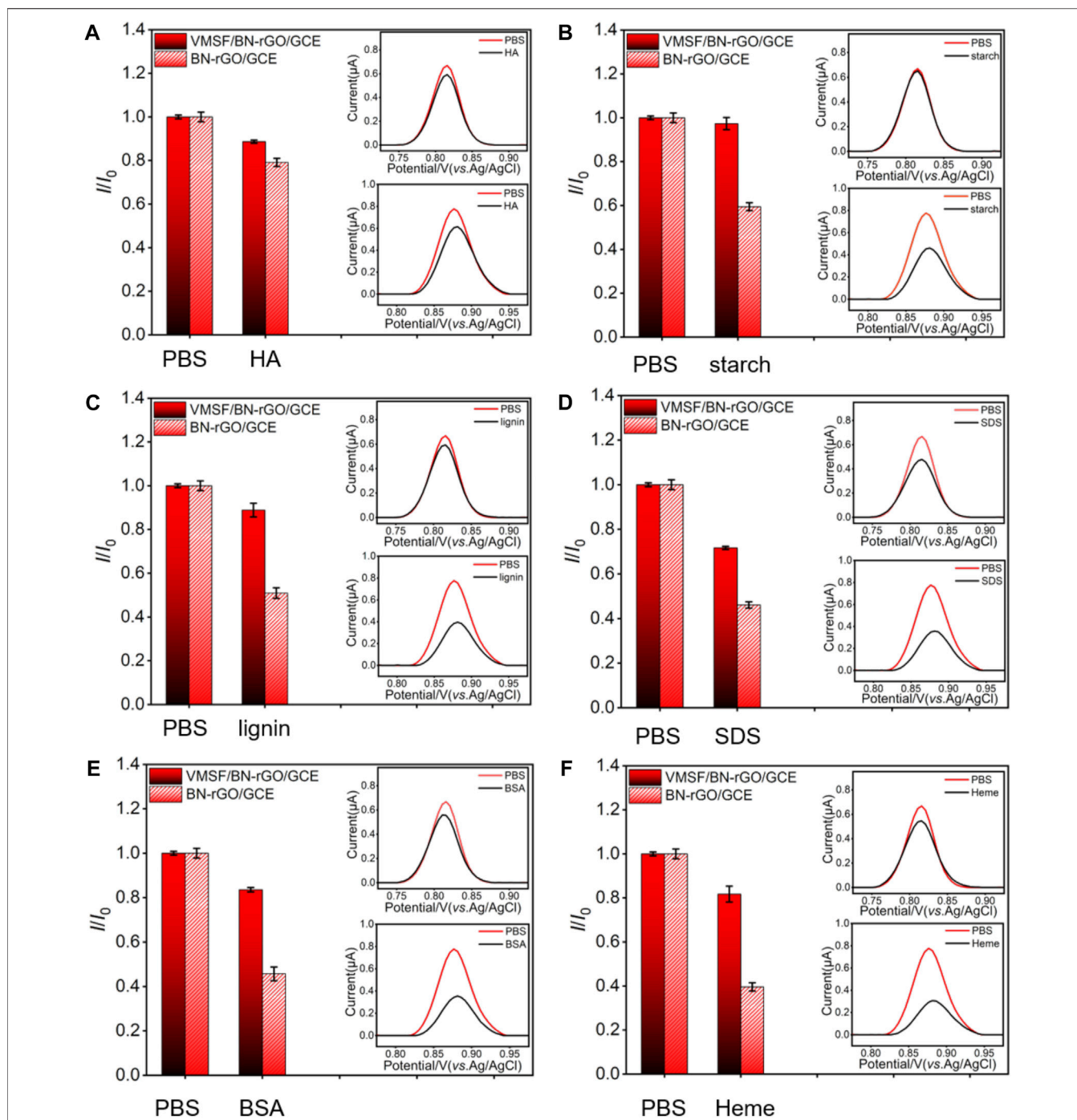
FIGURE 6 | Current ratio (I/I_0) obtained from VMSF/BN-rGO/GCE and BN-rGO/GCE for the detection of 1 μM CBZ in 0.1 M PBS containing 50 μg/ml HA (A), starch (B), lignin (C), SDS (D), BSA (E), or Heme (F). Insets are corresponding DPV curves of VMSF/BN-rGO/GCE (red line) and BN-rGO/GCE (black line) in the absence (top) or presence (bottom) of fouling species. The error bars represent the SD of three measurements.

(Cui et al., 2017). After modification of rGO on the GCE electrode, remarkably increased current signals are observed at the rGO/GCE, suggesting the good electrocatalytic activity of rGO. The introduction of BN into the rGO nanosheets could further enhance the current signals, indicating the higher electrocatalytic activity of the BN-rGO composite. Due to the

enrichment effect of hydrogen bonds between the silanol groups of VMSF and secondary amine groups of CBZ, peak currents obtained at the VMSF/BN-rGO/GCE further increase. And the magnitude of oxidation peak current at the VMSF/BN-rGO/GCE is about 2-3-fold higher than that obtained at the rGO/GCE or BN-rGO/GCE and 30-fold higher than that obtained at the bare

TABLE 2 | Recovery of CBZ in diluted pond water and grape juice.

Sample	Added (μM)	Found (μM)	RSD (%)	Recovery (%)
Pond water	0.300	0.313	3.3	104
	1.00	0.976	0.7	97.6
	2.00	2.04	0.2	102
Grape juice	0.300	0.303	4.0	101
	1.00	0.963	2.0	96.3
	2.00	2.02	2.1	101

GCE (inset of **Figure 4A**). **Figure 4B** shows the CV curves of 1 μM CBZ at the VMSF/BN-rGO/GCE at various scan rates. As demonstrated, both oxidation and reduction peak currents have a good linear relationship with scan rate in the range of 80–320 mV s^{-1}, indicating the adsorption-controlled electrochemical process.

Optimization of Experimental Conditions

To achieve the optimal detection performance, the influences of pH value of supporting electrolyte and preconcentration time on the electrochemical detection of CBZ were studied. **Supplementary Figure. S1A** shows the DPV responses of the VMSF/BN-rGO/GCE to 1 μM CBZ in 0.1 M PBS at different pH values. With the pH increasing from 4.0 to 8.0, the oxidation peak shifts negatively and exists a favorable linear relationship with the pH (inset of **Supplementary Figure S1A**) with the slope of −62 mV/pH. This suggests that the electron transfer is accompanied by an equal number of protons in the redox reaction of CBZ at the VMSF/BN-rGO/GCE according to the Nernst equation (Ilager et al., 2021). Moreover, the maximal oxidation peak current is obtained at the pH of 6.0, which is used for subsequent detection of CBZ. Since mechanical stirring could accelerate the diffusion of CBZ to the underlying electrode surface along the nanochannels of VMSF, the influence of stirring time on detection performance was investigated. As displayed in **Supplementary Figure S2**, the oxidation peak current of CBZ at the VMSF/BN-rGO/GCE increases with the increasing stirring time and reaches a plateau at 4 min. Therefore, 4 min was employed as the best preconcentration time for the following study.

Electrochemical Determination of CBZ in Buffer Solution

Under optimal experimental conditions, VMSF/BN-rGO/GCE was utilized to detect CBZ with different concentrations and the results were shown in **Figure 5**. As can be seen, as the CBZ concentrations increase, the measured oxidation peak current signals increase gradually in the range from 5 nM to 7 μM. There is a good linear relationship between oxidation peak currents and CBZ concentration. And the obtained linear fitting equation was I (μA) = 3.70 C (μM)—0.0512 (R^2 = 0.997), with a limit of detection (LOD) of 2 nM. **Table 1** compares the analytical performances between the proposed VMSF/BN-rGO/GCE and other reported sensors for CBZ

detection. As presented, VMSF/BN-rGO/GCE has a relatively wide linear range and a lower LOD.

Anti-interference and Anti-fouling Performance

Due to the intrinsic anti-interference and anti-fouling capacities, we investigated the performance of the VMSF/BN-rGO/GCE by comparing the oxidation peak currents of CBZ in the absence and presence of various ions (CO_3^{2-}, PO_4^{3-}, Mg^{2+}, K^+ and Na^+) and biologically related species (HA, starch, lignin, SDS, BSA, and heme). The results shown in **Supplementary Figure S3** and **Figure 6** suggest that the presence of interferents has no obvious influence on the CBZ detection. Moreover, the anti-fouling performance of the VMSF/BN-rGO/GCE and BN-rGO/GCE was compared in **Figure 6**. As seen, BN-rGO/GCE has a much reduced oxidation peak current after the addition of biologically related species into the buffer solution. By contrast, VMSF/BN-rGO/GCE remains comparable signals for these six interfering species, indicating the great potential of VMSF/BN-rGO/GCE in complex samples. However, arising from the hydrolysis of VMSF, the proposed sensor could not be used in strong alkaline solutions for a long time.

Electrochemical Determination of CBZ in Real Samples

We selected pond water and grape juice as actual samples to investigate the feasibility of the sensor in practical application. The pond water (20-fold diluted) and grape juice (50-fold diluted) samples were only diluted by 0.1 M PBS (pH = 6.0) prior to determination. Then a series of CBZ solutions with known concentrations were added to the aforementioned diluted pond water and grape juice samples. By comparing the detected concentrations detected by VMSF/BN-rGO/GCE with the known concentrations, good recoveries, and low RSD values are observed at the VMSF/BN-rGO/GCE, proving that the proposed sensor can quantitatively detect CBZ in real samples.

CONCLUSION

In summary, we have reported a simple electrochemical method for highly sensitive detection of CBZ using the VMSF/BN-rGO/GCE sensor. A layered nanocomposite consisting of BN and rGO could act as a conductive and stabilized layer for the stable growth of VMSF by using the EASA method. Arising from the excellent electrocatalytic performance of BN-rGO nanocomposite and the good anti-fouling capacity, the proposed VMSF/BN-rGO/GCE sensor can realize the direct and highly sensitive detection of CBZ in complex sample of pond water and grape juice samples. Integration with flexible electrodes and wireless devices will make the present sensor more useful in environmental monitoring and food quality control (**Table 2**).

DATA AVAILABILITY STATEMENT

The original contributions presented in the study are included in the article/**Supplementary Material**, further inquiries can be directed to the corresponding authors.

AUTHOR CONTRIBUTIONS

YZ, XZ, and LX curated the data. HT wrote and edited the manuscript. FY handled the supervision, reviewing, editing, and writing of the manuscript.

SUPPLEMENTARY MATERIAL

The Supplementary Material for this article can be found online at: https://www.frontiersin.org/articles/10.3389/fchem.2022.939510/full#supplementary-material

REFERENCES

Akilarasan, M., Kogularasu, S., Chen, S.-M., Govindasamy, M., Chen, T.-W., Ali, M. A., et al. (2018). A Green Approach to the Synthesis of Well-Structured Prussian Blue Cubes for the Effective Electrocatalytic Reduction of Antiprotozoal Agent Coccidiostat Nicarbazin. *Electroanalysis* 30, 1669–1677. doi:10.1002/elan.201700750

Baigorria, E., and Fraceto, L. F. (2022). Novel Nanostructured Materials Based on Polymer/organic-Clay Composite Networks for the Removal of Carbendazim from Waters. *J. Clean. Prod.* 331, 129867. doi:10.1016/j.jclepro.2021.129867

Cui, R., Xu, D., Xie, X., Yi, Y., Quan, Y., Zhou, M., et al. (2017). Phosphorus-doped Helical Carbon Nanofibers as Enhanced Sensing Platform for Electrochemical Detection of Carbendazim. *Food Chem.* 221, 457–463. doi:10.1016/j.foodchem.2016.10.094

Cui, Y., Duan, W., Jin, Y., Wo, F., Xi, F., and Wu, J. (2020). Ratiometric Fluorescent Nanohybrid for Noninvasive and Visual Monitoring of Sweat Glucose. *ACS Sens.* 5, 2096–2105. doi:10.1021/acssensors.0c00718

Cui, Y., Duan, W., Jin, Y., Wo, F., Xi, F., and Wu, J. (2021). Graphene Quantum Dot-Decorated Luminescent Porous Silicon Dressing for Theranostics of Diabetic Wounds. *Acta Biomater.* 131, 544–554. doi:10.1016/j.actbio.2021.07.018

Du, M., Wu, Y., and Hao, X. (2013). A Facile Chemical Exfoliation Method to Obtain Large Size Boron Nitride Nanosheets. *CrystEngComm* 15, 1782–1786. doi:10.1039/c2ce26446c

Duan, W., Jin, Y., Cui, Y., Xi, F., Liu, X., Wo, F., et al. (2021). A Co-delivery Platform for Synergistic Promotion of Angiogenesis Based on Biodegradable, Therapeutic and Self-Reporting Luminescent Porous Silicon Microparticles. *Biomaterials* 272, 120772. doi:10.1016/j.biomaterials.2021.120772

Farooq, S., Nie, J., Cheng, Y., Bacha, S. A. S., and Chang, W. (2020). Selective Extraction of Fungicide Carbendazim in Fruits Using β-cyclodextrin Based Molecularly Imprinted Polymers. *J. Sep. Sci.* 43, 1145–1153. doi:10.1002/jssc.201901029

Furini, L. N., Sanchez-Cortes, S., López-Tocón, I., Otero, J. C., Aroca, R. F., and Constantino, C. J. L. (2015). Detection and Quantitative Analysis of Carbendazim Herbicide on Ag Nanoparticles via Surface-Enhanced Raman Scattering. *J. Raman Spectrosc.* 46, 1095–1101. doi:10.1002/jrs.4737

Gao, X., Gao, Y., Bian, C., Ma, H., and Liu, H. (2019). Electroactive Nanoporous Gold Driven Electrochemical Sensor for the Simultaneous Detection of Carbendazim and Methyl Parathion. *Electrochimica Acta* 310, 78–85. doi:10.1016/j.electacta.2019.04.120

Ge, S., He, J., Ma, C., Liu, J., Xi, F., and Dong, X. (2019). One-step Synthesis of Boron-doped Graphene Quantum Dots for Fluorescent Sensors and Biosensor. *Talanta* 199, 581–589. doi:10.1016/j.talanta.2019.02.098

Ghorbani, A., Ojani, R., Ganjali, M. R., and Raoof, J. (2021). Direct Voltammetric Determination of Carbendazim by Utilizing a Nanosized Imprinted Polymer/MWCNTs-Modified Electrode. *J. Iran. Chem. Soc.* 18, 3109–3118. doi:10.1007/s13738-021-02255-3

Gong, J., Zhang, Z., Zeng, Z., Wang, W., Kong, L., Liu, J., et al. (2021a). Graphene Quantum Dots Assisted Exfoliation of Atomically-Thin 2D Materials and As-Formed 0D/2D Van Der Waals Heterojunction for HER. *Carbon* 184, 554–561. doi:10.1016/j.carbon.2021.08.063

Gong, J., Tang, H., Luo, X., Zhou, H., Lin, X., Wang, K., et al. (2021b). Vertically Ordered Mesoporous Silica-Nanochannel Film-Equipped Three-Dimensional Macroporous Graphene as Sensitive Electrochemiluminescence Platform. *Front. Chem.* 9, 770512. doi:10.3389/fchem.2021.770512

Govindasamy, M., Mani, V., Chen, S. M., Chen, T. W., and Sundramoorthy, A. K. (2017a). Methyl Parathion Detection in Vegetables and Fruits Using Silver@graphene Nanoribbons Nanocomposite Modified Screen Printed Electrode. *Sci. Rep.* 7, 46571–46582. doi:10.1038/srep46471

Govindasamy, M., Chen, S.-M., Mani, V., Devasenathipathy, R., Umamaheswari, R., Joseph Santhanaraj, K., et al. (2017b). Molybdenum Disulfide Nanosheets Coated Multiwalled Carbon Nanotubes Composite for Highly Sensitive Determination of Chloramphenicol in Food Samples Milk, Honey and Powdered Milk. *J. Colloid Interface Sci.* 485, 129–136. doi:10.1016/j.jcis.2016.09.029

Grujic, S., Radisic, M., Vasiljevic, T., and Lausevic, M. (2005). Determination of Carbendazim Residues in Fruit Juices by Liquid Chromatography-Tandem Mass Spectrometry. *Food Addit. Contam.* 22, 1132–1137. doi:10.1080/02652030500352863

He, J., Li, Z., Zhao, R., Lu, Y., Shi, L., Liu, J., et al. (2019). Aqueous Synthesis of Amphiphilic Graphene Quantum Dots and Their Application as Surfactants for Preparing of Fluorescent Polymer Microspheres. *Colloids Surfaces A Physicochem. Eng. Aspects* 563, 77–83. doi:10.1016/j.colsurfa.2018.11.064

Huang, B., He, J., Bian, S., Zhou, C., Li, Z., Xi, F., et al. (2018). S-doped Graphene Quantum Dots as Nanophotocatalyst for Visible Light Degradation. *Chin. Chem. Lett.* 29, 1698–1701. doi:10.1016/j.cclet.2018.01.004

Huaxu Zhou, H., Ding, Y., Su, R., Lu, D., Tang, H., and Xi, F. (2021). Silica Nanochannel Array Film Supported by SS-Cyclodextrin-Functionalized Graphene Modified Gold Film Electrode for Sensitive and Direct Electroanalysis of Acetaminophen. *Front. Chem.* 9, 812086. doi:10.3389/fchem.2021.812086

Ilager, D., Seo, H., Kalanur, S. S., Shetti, N. P., and Aminabhavi, T. M. (2021). A Novel Sensor Based on WO3·0.33H2O Nanorods Modified Electrode for the Detection and Degradation of Herbicide, Carbendazim. *J. Environ. Manag.* 279, 111611. doi:10.1016/j.jenvman.2020.111611

Kaixin Li, K., Chen, J., Yan, Y., Min, Y., Li, H., Xi, F., et al. (2018). Quasi-homogeneous Carbocatalysis for One-Pot Selective Conversion of Carbohydrates to 5-hydroxymethylfurfural Using Sulfonated Graphene Quantum Dots. *Carbon* 136, 224–233. doi:10.1016/j.carbon.2018.04.087

Keerthi, M., Akilarasan, M., Chen, S.-M., Kogularasu, S., Govindasamy, M., Mani, V., et al. (2018). One-Pot Biosynthesis of Reduced Graphene Oxide/Prussian Blue Microcubes Composite and its Sensitive Detection of Prophylactic Drug Dimetridazole. *J. Electrochem. Soc.* 165, B27–B33. doi:10.1149/2.0591802jes

Kogularasu, S., Govindasamy, M., Chen, S.-M., Akilarasan, M., and Mani, V. (2017). 3D Graphene Oxide-Cobalt Oxide Polyhedrons for Highly Sensitive Non-enzymatic Electrochemical Determination of Hydrogen Peroxide. *Sensors Actuators B Chem.* 253, 773–783. doi:10.1016/j.snb.2017.06.172

Lesueur, C., Gartner, M., Mentler, A., and Fuerhacker, M. (2008). Comparison of Four Extraction Methods for the Analysis of 24 Pesticides in Soil Samples with Gas Chromatography-Mass Spectrometry and Liquid Chromatography-Ion Trap-Mass Spectrometry. *Talanta* 75, 284–293. doi:10.1016/j.talanta.2007.11.031

Lin Zhou, L., Li, X., Zhu, B., and Su, B. (2021). An Overview of Antifouling Strategies for Electrochemical Analysis. *Electroanal* 33, 1–11. doi:10.1002/elan. 202100406

Liu, X., Chen, Z., Wang, T., Jiang, X., Qu, X., Duan, W., et al. (2022). Tissue Imprinting on 2D Nanoflakes-Capped Silicon Nanowires for Lipidomic Mass Spectrometry Imaging and Cancer Diagnosis. *ACS Nano* 16, 6916–6928. doi:10.1021/acsnano.2c02616

Lu, L., Zhou, L., Chen, J., Yan, F., Liu, J., Dong, X., et al. (2018). Nanochannel-Confined Graphene Quantum Dots for Ultrasensitive Electrochemical Analysis of Complex Samples. *ACS Nano* 12, 12673–12681. doi:10.1021/acsnano.8b07564

Ma, K., Yang, L., Liu, J., and Liu, J. (2022a). Electrochemical Sensor Nanoarchitectonics for Sensitive Detection of Uric Acid in Human Whole Blood Based on Screen-Printed Carbon Electrode Equipped with Vertically-Ordered Mesoporous Silica-Nanochannel Film. *Nanomaterials* 12, 1157. doi:10.3390/nano12071157

Ma, K., Zheng, Y., An, L., and Liu, J. (2022b). Ultrasensitive Immunosensor for Prostate-specific Antigen Based on Enhanced Electrochemiluminescence by Vertically Ordered Mesoporous Silica-Nanochannel Film. *Front. Chem.* 10, 851178. doi:10.3389/fchem.2022.851178

Mao, Y., Zhao, C., Ge, S., Luo, T., Chen, J., Liu, J., et al. (2019). Gram-scale Synthesis of Nitrogen Doped Graphene Quantum Dots for Sensitive Detection of Mercury Ions and L-Cysteine. *RSC Adv.* 9, 32977–32983. doi:10.1039/c9ra06113d

Mekeuo, G., Despas, C., Nanseu-Njiki, C., Walcarius, A., and Ngameni, E. (2021). Preparation of Functionalized Ayous Sawdust-Carbon Nanotubes Composite for the Electrochemical Determination of Carbendazim Pesticide. *Electroanal* 33, 1–11. doi:10.1002/elan.202100262

Muthumariappan, A., Govindasamy, M., Chen, S.-M., Sakthivel, K., and Mani, V. (2017). Screen-printed Electrode Modified with a Composite Prepared from Graphene Oxide Nanosheets and Mn3O4 Microcubes for Ultrasensitive Determination of Nitrite. *Microchim. Acta* 184, 3625–3634. doi:10.1007/s00604-017-2379-9

Nan Li, N., Than, A., Chen, J., Xi, F., Liu, J., and Chen, P. (2018). Graphene Quantum Dots Based Fluorescence Turn-On Nanoprobe for Highly Sensitive and Selective Imaging of Hydrogen Sulfide in Living Cells. *Biomater. Sci.* 6, 779–784. doi:10.1039/c7bm00818j

Nasir, T., Herzog, G., Hébrant, M., Despas, C., Liu, L., and Walcarius, A. (2018). Mesoporous Silica Thin Films for Improved Electrochemical Detection of Paraquat. *ACS Sens.* 3, 484–493. doi:10.1021/acssensors.7b00920

Özcan, A., Hamid, F., and Özcan, A. A. (2021). Synthesizing of a Nanocomposite Based on the Formation of Silver Nanoparticles on Fumed Silica to Develop an Electrochemical Sensor for Carbendazim Detection. *Talanta* 222, 121591. doi:10.1016/j.talanta.2020.121591

Pang, Y., Zhao, R., Lu, Y., Liu, J., Dong, X., and Xi, F. (2018). Facile Preparation of N-Doped Graphene Quantum Dots as Quick-Dry Fluorescent Ink for Anti-counterfeiting. *New J. Chem.* 42, 17091–17095. doi:10.1039/c8nj03375g

Phansawan, B., Prapamontol, T., Thavornyutikarn, P., Chantara, S., Mangklabruks, A., and Santasup, C. (2015). A Sensitive Method for Determination of Carbendazim Residue in Vegetable Samples Using HPLC-UV and its Application in Health Risk Assessment. *Chiang Mai J. Sci.* 42, 681–690.

Pourreza, N., Rastegarzadeh, S., and Larki, A. (2015). Determination of Fungicide Carbendazim in Water and Soil Samples Using Dispersive Liquid-Liquid Microextraction and Microvolume UV-Vis Spectrophotometry. *Talanta* 134, 24–29. doi:10.1016/j.talanta.2014.10.056

Qun Li, Q., Huo, C., Yi, K., Zhou, L., Su, L., and Hou, X. (2018). Preparation of Flake Hexagonal BN and its Application in Electrochemical Detection of Ascorbic Acid, Dopamine and Uric Acid. *Sensors Actuators B Chem.* 260, 346–356. doi:10.1016/j.snb.2017.12.208

Rai, B., and Mercurio, S. D. (2020). Environmentally Relevant Exposures of Male Mice to Carbendazim and Thiram Cause Persistent Genotoxicity in Male Mice. *Environ. Sci. Pollut. Res.* 27, 10629–10641. doi:10.1007/s11356-019-07088-5

Subhani, Q., Huang, Z., Zhu, Z., and Zhu, Y. (2013). Simultaneous Determination of Imidacloprid and Carbendazim in Water Samples by Ion Chromatography with Fluorescence Detector and Post-column Photochemical Reactor. *Talanta* 116, 127–132. doi:10.1016/j.talanta.2013.05.023

Tian, J., Chen, J., Liu, J., Tian, Q., and Chen, P. (2018). Graphene Quantum Dot Engineered Nickel-Cobalt Phosphide as Highly Efficient Bifunctional Catalyst for Overall Water Splitting. *Nano Energy* 48, 284–291. doi:10.1016/j.nanoen.2018.03.063

Tian, C., Zhang, S., Wang, H., Chen, C., Han, Z., Chen, M., et al. (2019). Three-Dimensional Nanoporous Copper and Reduced Graphene Oxide Composites as Enhanced Sensing Platform for Electrochemical Detection of Carbendazim. *J. Electroanal. Chem.* 847, 113243. doi:10.1016/j.jelechem.2019.113243

Walcarius, A. (2021). Electroinduced Surfactant Self-Assembly Driven to Vertical Growth of Oriented Mesoporous Films. *Acc. Chem. Res.* 54, 3563–3575. doi:10.1021/acs.accounts.1c00233

Wan, Y., Zhao, J., Deng, X., Chen, J., Xi, F., and Wang, X. (2021). Colorimetric and Fluorescent Dual-Modality Sensing Platform Based on Fluorescent Nanozyme. *Front. Chem.* 9, 774486. doi:10.3389/fchem.2021.774486

Wang, W., Deng, P., Liu, X., Ma, Y., and Yan, Y. (2021). A CsPbBr3 Quantum Dots/ultra-Thin BN Fluorescence Sensor for Stability and Highly Sensitive Detection of Tetracycline. *Microchem. J.* 162, 105876. doi:10.1016/j.microc.2020.105876

Wang, K., Yang, L., Huang, H., Lv, N., Liu, J., and Liu, Y. (2022). Nanochannel Array on Electrochemically Polarized Screen Printed Carbon Electrode for Rapid and Sensitive Electrochemical Determination of Clozapine in Human Whole Blood. *Molecules* 27, 2739. doi:10.3390/molecules27092739

Wei, P., Gan, T., and Wu, K. (2018). N-methyl-2-pyrrolidone Exfoliated Graphene as Highly Sensitive Analytical Platform for Carbendazim. *Sensors Actuators B Chem.* 274, 551–559. doi:10.1016/j.snb.2018.07.174

Wei, X., Luo, X., Xu, S., Xi, F., and Zhao, T. (2022). A Flexible Electrochemiluminescence Sensor Equipped with Vertically Ordered Mesoporous Silica Nanochannel Film for Sensitive Detection of Clindamycin. *Front. Chem.* 10, 872582. doi:10.3389/fchem.2022.872582

Weng, Q., Wang, X., Wang, X., Bando, Y., and Golberg, D. (2016). Functionalized Hexagonal Boron Nitride Nanomaterials: Emerging Properties and Applications. *Chem. Soc. Rev.* 45, 3989–4012. doi:10.1039/c5cs00869g

Xi, F., Xuan, L., Lu, L., Huang, J., Yan, F., Liu, J., et al. (2019). Improved Adhesion and Performance of Vertically-Aligned Mesoporous Silica-Nanochannel Film on Reduced Graphene Oxide for Direct Electrochemical Analysis of Human Serum. *Sensors Actuators B Chem.* 288, 133–140. doi:10.1016/j.snb.2019.02.115

Xuan, L., Liao, W., Wang, M., Zhou, H., Ding, Y., Yan, F., et al. (2021). Integration of Vertically-Ordered Mesoporous Silica-Nanochannel Film with Electro-Activated Glassy Carbon Electrode for Improved Electroanalysis in Complex Samples. *Talanta* 225, 122066. doi:10.1016/j.talanta.2020.122066

Yamaguchi, A., Namekawa, M., Kamijo, T., Itoh, T., and Teramae, N. (2011). Acid–Base Equilibria inside Amine-Functionalized Mesoporous Silica. *Anal. Chem.* 83, 2939–2946. doi:10.1021/ac102935q

Yan, Y., Chen, J., Li, N., Tian, J., Li, K., Jiang, J., et al. (2018). Systematic Bandgap Engineering of Graphene Quantum Dots and Applications for Photocatalytic Water Splitting and CO2 Reduction. *ACS Nano* 12, 3523–3532. doi:10.1021/acsnano.8b00498

Yan, Y., Gong, J., Chen, J., Zeng, Z., Huang, W., Pu, K., et al. (2019). Recent Advances on Graphene Quantum Dots: From Chemistry and Physics to Applications. *Adv. Mater* 31, e1808283. doi:10.1002/adma.201808283

Yan, F., Chen, J., Jin, Q., Zhou, H., Sailjoi, A., Liu, J., et al. (2020a). Fast One-step Fabrication of a Vertically-Ordered Mesoporous Silica-Nanochannel Film on Graphene for Direct and Sensitive Detection of Doxorubicin in Human Whole Blood. *J. Mat. Chem. C* 8, 7113–7119. doi:10.1039/d0tc00744g

Yan, F., Ma, X., Jin, Q., Tong, Y., Tang, H., Lin, X., et al. (2020b). Phenylboronic Acid-Functionalized Vertically Ordered Mesoporous Silica Films for Selective Electrochemical Determination of Fluoride Ion in Tap Water. *Microchim. Acta* 187, 470. doi:10.1007/s00604-020-04422-4

Yan, F., Luo, T., Jin, Q., Zhou, H., Sailjoi, A., Dong, G., et al. (2021). Tailoring Molecular Permeability of Vertically-Ordered Mesoporous Silica-Nanochannel Films on Graphene for Selectively Enhanced Determination of Dihydroxybenzene Isomers in Environmental Water Samples. *J. Hazard. Mater.* 410, 124636. doi:10.1016/j.jhazmat.2020.124636

Yan, F., and Su, B. (2016). Tailoring Molecular Permeability of Nanochannel-Micelle Membranes for Electrochemical Analysis of Antioxidants in Fruit Juices without Sample Treatment. *Anal. Chem.* 88, 11001–11006. doi:10.1021/acs.analchem.6b02823

Yang, Y., Huo, D., Wu, H., Wang, X., Yang, J., Bian, M., et al. (2018). N, P-Doped Carbon Quantum Dots as a Fluorescent Sensing Platform for Carbendazim

Detection Based on Fluorescence Resonance Energy Transfer. *Sensors Actuators B Chem.* 274, 296–303. doi:10.1016/j.snb.2018.07.130

Yang, Y., Xing, X., Zou, T., Wang, Z., Zhao, R., Hong, P., et al. (2020). A Novel and Sensitive Ratiometric Fluorescence Assay for Carbendazim Based on N-Doped Carbon Quantum Dots and Gold Nanocluster Nanohybrid. *J. Hazard. Mater.* 386, 121958. doi:10.1016/j.jhazmat.2019.121958

Zhou, L., Ding, H., Yan, F., Guo, W., and Su, B. (2018). Electrochemical Detection of Alzheimer's Disease Related Substances in Biofluids by Silica Nanochannel Membrane Modified Glassy Carbon Electrodes. *Analyst* 143, 4756–4763. doi:10.1039/c8an01457d

Zhou, P., Yao, L., Chen, K., and Su, B. (2019). Silica Nanochannel Membranes for Electrochemical Analysis and Molecular Sieving: A Comprehensive Review. *Crit. Rev. Anal. Chem.* 50, 1–21. doi:10.1080/10408347.2019.1642735

Zhou, P., Yao, L., Chen, K., and Su, B. (2020). Silica Nanochannel Membranes for Electrochemical Analysis and Molecular Sieving: A Comprehensive Review. *Crit. Rev. Anal. Chem.* 50, 424–444. doi:10.1080/10408347.2019.1642735

Zhou, H., Ma, X., Sailjoi, A., Zou, Y., Lin, X., Yan, F., et al. (2022). Vertical Silica Nanochannels Supported by Nanocarbon Composite for Simultaneous Detection of Serotonin and Melatonin in Biological Fluids. *Sensors Actuators B Chem.* 353, 131101. doi:10.1016/j.snb.2021.131101

Zhu, C., Liu, D., Chen, Z., Li, L., and You, T. (2019). An Ultra-sensitive Aptasensor Based on Carbon Nanohorns/gold Nanoparticles Composites for Impedimetric Detection of Carbendazim at Picogram Levels. *J. Colloid Interface Sci.* 546, 92–100. doi:10.1016/j.jcis.2019.03.035

Zhu, X., Xuan, L., Gong, J., Liu, J., Wang, X., Xi, F., et al. (2022). Three-dimensional Macroscopic Graphene Supported Vertically-Ordered Mesoporous Silica-Nanochannel Film for Direct and Ultrasensitive Detection of Uric Acid in Serum. *Talanta* 238, 123027. doi:10.1016/j.talanta.2021.123027